

Scaling of the velocity profile in strongly drag reduced turbulent flows over an oscillating wall

Martin Skote^{a,*}

^a *School of Mechanical & Aerospace Engineering
Nanyang Technological University
50 Nanyang Avenue, Singapore 639798*

Abstract

Scaling analysis of the velocity profiles in strongly drag reduced flows reveals that the slope of the logarithmic part depends on the amount of drag reduction (DR). Unlike DR due to polymeric fluids, the slope changes gradually and can be predicted by the analysis. Furthermore, the intercept of the profiles is found to vary linearly with the DR. Two velocity scales are utilized: the reference (undisturbed) and the actual friction velocity. The theory is based on the assumption that the near-wall linear region is only governed by the actual friction velocity, while the outer part is governed by the reference friction velocity. As a result, logarithmic part is influenced by both velocity scales and the slope of the velocity profile is directly linked to the DR. The theoretically obtained results are verified by data from six previously performed direct numerical simulations (DNSs) of boundary layers over spatial and temporal wall oscillations, with a wide range of resulting DR. The theory is further supported by data from numerous investigations (DNSs as well as experiments) of wall-bounded flows forced by various forms of oscillating wall-motion. The assumption that the outer part is unaffected by the actual friction velocity limits the validity of the proposed log-law to flows not fully adapted to the imposed wall forcing, hence the theory provides a measure of the level of adjustment. In addition, a fundamental difference in the applicability of the theory to spatially developing boundary flow and infinite channel flow is discussed.

Keywords: Turbulent Boundary Layer, Oscillating Wall, Drag Reduction, Velocity profile

1. Introduction

Many methods for reducing the viscous drag of turbulent flows over a wall have been proposed through the years. From a control strategy point of view,

*Corresponding author
Email address: mskote@ntu.edu.sg. (Martin Skote)

most methods are based on an open loop concept, i.e. no sensor feedback is involved. Examples include introducing polymer solution (White and Mungal, 2008; Tamano et al., 2011) or air bubbles (Elbing et al., 2013), in the case of liquid flow. For boundary layers in air, however, the most viable technique is to change the surface, either the morphology of the wall (passive control), or impose a motion of the wall or fluid (active control). One example of the former is based on riblets (García-Mayoral and Jiménez, 2011), which is a method motivated by the practicality and aims at being directly implementable. The penalty is that the drag reduction (DR) is not great, typically less than 10% for riblets. Other methods based on a dynamic manipulation of the wall which, even though not easily applicable to in a real engineering framework, have provided much greater drag reduction (Karniadakis and Choi, 2003). So far, these manipulations either consist of temporal/spatial spanwise oscillations (Quadrio, 2011) of the wall, or a morphological deformation of the surface (Nakanishi et al., 2012). Promising results have also been demonstrated by blowing and suction of fluid through the wall (Min et al., 2006).

In this paper certain aspects of the velocity profile which are detectable only at large values of DR will be discussed. In addition, the study is limited to flows where the DR is obtained via various forms of oscillating motion as the mode of wall forcing. The reason for this limitation is that methods based on altering the fluid properties, such as polymeric fluid, affects the turbulence throughout the domain, see e.g. Virk (1975), and is not limited to near-wall effects. In addition, the mechanism behind DR is much more complex due to non-Newtonian effects for these types of fluids. For the most recent theoretical development of the analysis of polymer drag reduced flow, see White et al. (2012).

A large number of DNSs and experiments of wall-bounded turbulent flows with oscillating walls exists, see e.g. Skote (2013) and references therein. However, previous studies have all focused on attempts to systematically study either energy budgets or flow structures, respectively, as means of explaining the DR mechanisms. Regarding the velocity profiles, most studies have limited themselves to observations which can be summarized in the following points:

- Scaled with actual friction velocity:
 - the linear profile is retained.
 - the logarithmic profile is shifted upward.
- Scaled with the reference friction velocity:
 - the self-similarity in the linear region is lost.
 - the logarithmic profile is shifted slightly upward.

While most investigations have concluded this behaviour, no thorough and systematic analysis has been attempted. In the present work, the properties of the velocity profiles described above will be quantified and amended with the important feature that apart from the upward shift of the logarithmic part, also

the slope is altered, when scaled with actual friction velocity. However, this behaviour is most noticeable for very high degrees of DR, and therefore DNS data from previously performed simulations of boundary layer with DR in the range of 18% - 46% will be used. Additional data which confirm the findings are taken from experiments by Choi and Clayton (2001) and Ricco and Wu (2004) of boundary layer flow and DNSs by Touber and Leschziner (2012) and Quadrio et al. (2009) of channel flow. The change in the slope of the logarithmic part of the velocity profile has been observed for DR generating polymeric fluids. However, the behaviour is different from the case of wall oscillation induced DR. As described by White and Mungal (2008), the log profile in the polymeric case remains parallel to the unmanipulated case until the DR reaches 40% after which the slope increases. In contrast, the slope in the case of wall oscillations is gradually increasing and is directly related to the amount of DR, which will be demonstrated in the present paper using analysis, DNS data, and experimental data.

The results presented here may be important from two points of view. First, the various groups currently working on the drag reduction techniques will be able to compare their velocity profiles with the theory provided. Second, researchers developing tools based on turbulence modelling for predicting the efficiency of various drag reduction techniques will find the theoretical aspects presented here valuable. Although such tools have recently started to emerge, see e.g. the work by Duque-Daza et al. (2012) or Moarref and Jovanović (2012), it is my hope that the findings described in this paper will speed-up the model development process.

The remaining part of the paper is structured as follows. In Section 2 the analysis of the logarithmic and inner part of the boundary layer velocity profiles is presented. The results are compared with a set of six DNSs of boundary layer flow with DR produced by temporal and spatial wall oscillations in Section 3. In Section 4 further confirmation by utilizing data from boundary layer experiments as well as DNS of channel flow at various Reynolds numbers (Re) and with different mode of DR techniques is provided. The range of applicability of the theory is discussed in Section 5 before the conclusions are summarized in Section 6.

2. Analysis

In the following, two velocity scales will be used, namely the friction velocity of the unmanipulated boundary layer (the reference case), denoted u_τ^0 , and the actual friction velocity (u_τ). The friction velocity is defined as

$$u_\tau \equiv \sqrt{\nu \left. \frac{\partial u}{\partial y} \right|_{y=0}} \quad (1)$$

where ν is the kinematic viscosity.

The DR will in this paper be quantified according to:

$$\mathcal{D} = \frac{C_f^0 - C_f}{C_f^0}, \quad (2)$$

where $C_f^0 = 2(u_\tau^0/u_\infty)^2$ is the skin friction of the reference case. Hence, we may write $\mathcal{D} = 1 - r^2$, where r is the ratio between the two velocity scales, $r = u_\tau/u_\tau^0$.

The logarithmic behaviour of the turbulent boundary layer is obtained from the asymptotic matching of the velocity gradient in the inner and outer regions of the boundary layer. In the following we will utilize the knowledge that the velocity profile in the inner part is completely governed by u_τ while the wake function or velocity defect (and hence also the velocity gradient) in the outer part is completely governed by u_τ^0 . The argument for the latter scaling proposition is that the outer part is not affected by the change of velocity scale near the wall where the wall manipulations generate the DR. Hence the classical theory (Clauser, 1956) of wall manipulated boundary layer flow is followed in the sense that the wake function is assumed to be unaffected. As will be shown below, the classical theory is however expanded with the permission of a change of the von Kármán coefficient (or rather, the slope of the logarithmic velocity profile). This is also the reason why the theory can only be applied to flows where the control is imposed through wall manipulation, since changing the fluid properties by polymers or by other means clearly affects the flow also far away from the wall. In the procedure below, the analytical steps demonstrated by Skote and Henningson (2002) are followed.

At this point it is necessary to define the notation for the scaling by two different velocity scales. For the vertical coordinate (y) we will use $y^+ \equiv yu_\tau/\nu$ and $y_0^+ \equiv yu_\tau^0/\nu$, while the streamwise velocity (u) is written as $u^+ \equiv u/u_\tau$ and $u_0^+ \equiv u/u_\tau^0$.

For the matching of the inner and outer equations, it is enough to observe that the velocity gradient can be written in the following form in the inner part:

$$\frac{\partial u}{\partial y} = f' u_\tau^2 / \nu, \quad (3)$$

where f' is a function of a similarity variable (y^+).

In the outer part it is assumed that the velocity gradient can be written,

$$\frac{\partial u}{\partial y} = F' u_\tau^0 / \Delta, \quad (4)$$

where F' is a function of a similarity variable ($\eta \equiv y/\Delta$) and Δ is the outer length scale.

The crucial step here is the use of u_τ for the inner part, and u_τ^0 for the outer part. If the assumptions (3) and (4) are valid, then the matching of the velocity gradient gives the equation,

$$f' y^+ r = F' \eta, \quad (5)$$

where r is the ratio between the two velocity scales,

$$r = \frac{u_\tau}{u_\tau^0} = \sqrt{1 - \mathcal{D}}. \quad (6)$$

Noting that the two sides of (5) depend on different variables, we set the first part equal to a constant and formulate it as,

$$y^+ \frac{du^+}{dy^+} = \frac{1}{\kappa r}. \quad (7)$$

In the reference case, $r = 1$ and Eq. (7) yields the usual logarithmic velocity profile when integrated:

$$u^+ = \frac{1}{\kappa} \ln y^+ + B_0. \quad (8)$$

with $\kappa = 0.41$ and $B_0 = 5.2$. For the case with DR, r is not equal to unity, and integrating Eq. (7) gives:

$$u^+ = \frac{1}{\kappa \sqrt{1 - \mathcal{D}}} \ln y^+ + B(\mathcal{D}). \quad (9)$$

From expression (9) it is evident that the slope of the log layer depends on the amount of DR.

If, on the other hand, the velocity profile is scaled with u_τ^0 , the logarithmic profile is simply obtained by multiplying (9) by r , followed by a change of variable from y^+ to $y_0^+ = y^+/r$, producing:

$$u_0^+ = \frac{1}{\kappa} \ln y_0^+ + \frac{1}{\kappa} \ln r + rB(\mathcal{D}). \quad (10)$$

Thus, the logarithmic part of the velocity profile can be scaled by either u_τ or u_τ^0 , yielding profiles (9) and (10), respectively, which both depend on the ratio (r) between the two velocity scales. Only the first case (scaling with u_τ) produce profiles with a slope depending on the DR, i.e. \mathcal{D} .

After the evaluation of the logarithmic part, we turn our attention to the near-wall region. The viscous sub-layer is governed by u_τ only, and hence this scaling produces the self-similar profiles obeying,

$$u^+ = y^+ \quad (11)$$

This linear relation originates from the integration of the governing equation for the viscous sub-layer:

$$0 = \nu \frac{\partial^2 u}{\partial^2 y} \quad (12)$$

which when integrated twice and utilizing the definition of u_τ yields (11). When scaling u and y with u_τ^0 instead, the integration described above yields,

$$u_0^+ = r^2 y_0^+, \quad (13)$$

which is a profile depending on r and hence is not self-similar.

3. Comparison with boundary layer DNS

In order to compare the theory described above with DNS and experiments, relatively high DR cases will be valuable as the change of slope of the log-layer will only be detected for those cases. In addition, since the theory is based on the assumption that the outer wake region is unaffected, only control based on wall manipulations can be considered. Previous investigations with these requirements fulfilled have focused on two different types of wall movements. In the first kind, temporal forcing, the wall oscillation is imposed through a wall velocity (W) in the spanwise direction in the form of

$$W = W_m \sin(\omega t), \quad (14)$$

where W_m is the maximum wall velocity and ω is the angular frequency of the wall oscillation, which is related to the period (T) through $\omega = 2\pi/T$. The second kind, which consists of a steady variation in the streamwise direction along the plate, the wall velocity (W) is imposed in the form of

$$W = W_m \sin(\kappa x), \quad (15)$$

where κ is the wavenumber of the spatial oscillation, which is related to the wavelength (λ_x) through $\kappa = 2\pi/\lambda_x$.

In the present paper results are first presented from previously reported DNSs of boundary layer flow with a temporally oscillating spanwise wall velocity according to Eq. (14) and a spatially oscillating spanwise wall velocity according to Eq. (15). Results from six different cases with widely varying DR are used to evaluate the scaling analysis. The cases are summarized in Table 1 together with the references to the original works where the numerical method is described. Here, the + superscript indicates that the quantity is made non-dimensional with the friction velocity (u_τ) at the start of the oscillations, and the kinematic viscosity (ν). All the simulations were performed at $Re_\Theta = 505$ (where Θ denotes momentum loss thickness), measured at the onset of wall forcing. The reference boundary layer has a Re_Θ of 750 at the end of the computational domain (corresponding to $Re_\tau = 300$ in a channel flow geometry). The simulations are thus performed with relatively short (in the streamwise direction) domains, hence no Reynolds number dependence can be investigated in the statistics. However, as shown by Skote (2012), the spatial transients (which can be related to the temporal transients in a channel flow geometry) has been properly accounted for in the simulations. Note that the spatial/temporal transients discussed here are related to the skin friction and hence the turbulence in the inner part of the boundary layer.

The velocity profiles from the region of constant DR (after the spatial transients have died out) are similar regardless of which streamwise position is chosen. Thus, it may be concluded that the simulations are long enough for spatial transients to vanish, but too short for any downstream development to be observed. The data used here are averaged over the spatial extent of approximately constant DR in order to remove any ambiguities.

Case	W_m^+	λ_x^+	T^+	\mathcal{D}	symbol	line
reference	0	0	0	0	*	—
1	6	0	132	0.18	◇	...
2	12	0	132	0.29	+	...
3	17	0	118	0.37	□	...
4	6	1320	0	0.25	▽	
5	12	1320	0	0.41	×	--
6	17	1300	0	0.46	○	--

Table 1: Summary of the cases investigated. Symbols and lines are used in Figs. 1 to 4. Cases 1 and 2 are taken from Skote (2012), case 3 is taken from Yudhistira and Skote (2011), cases 4 and 5 are taken from Skote (2013), and case 6 is taken from Skote (2011).

The velocity profiles from all six cases (together with the reference case) are shown in Fig. 1. Here the actual friction velocity (u_τ), is used to reveal that indeed this scaling yields a perfect collapse of the profile in the linear sub-layer. However, the velocity profiles in the logarithmic region are far from each other and the slope of the profiles changes with the amount of DR.

The straight lines with DR dependent slopes produced by (9) are shown in Fig. 1 together with the DNS data. The theoretically obtained slope ($1/\kappa r$) coincides with the DNS data. Hence, in contrast to the case of polymeric fluid induced DR, we can in this case of drag reduced flow predict the slope of the log layer.

Observe that the additive constant B in (9) is a function of the DR, i.e. \mathcal{D} . To illustrate this, B evaluated in Fig. 1 for each case is plotted in Fig. 2 as a function of \mathcal{D} . Interestingly, a linear relation is observed and obeys,

$$B(\mathcal{D}) = B_0 + k_D \mathcal{D} \quad (16)$$

with $k_D = 9.0$. The connection between the DR and shift upward of the velocity profile is of course nothing new since it has been observed for a long time. In fact, simplified relations between the shift and the DR, based on various degree of approximations, have been proposed from which k_D in equation (16) can be derived. For example, Luchini (1996) derived an expression which yields $k_D = (2C_f^0)^{-1/2} + (2\kappa)^{-1}$. This expression can also be found in García-Mayoral and Jiménez (2011). Spalart and McLean (2011) use a slightly different approach and arrives at $k_D = (2C_f^0)^{-1/2}$. These two expressions give the value of 10.3 and 11.5, respectively, for k_D . However, since the theoretical derivations are based on linearization and is only valid for relatively small values of the DR, the applicability to the present high-DR cases is questionable.

When scaled with u_τ^0 the profiles are parallel (the slope is $1/\kappa$ regardless of \mathcal{D}) as indicated by (10). In addition, the profiles are closer to each other, and therefore only the most extreme case (case 6) is shown in Fig. 3. Again, the theoretically obtained profiles fall on the DNS data. Note that identical values of B as found in the first scaling are used for all six profiles, and all cases show equally good collapse of the profiles as for the case 6.

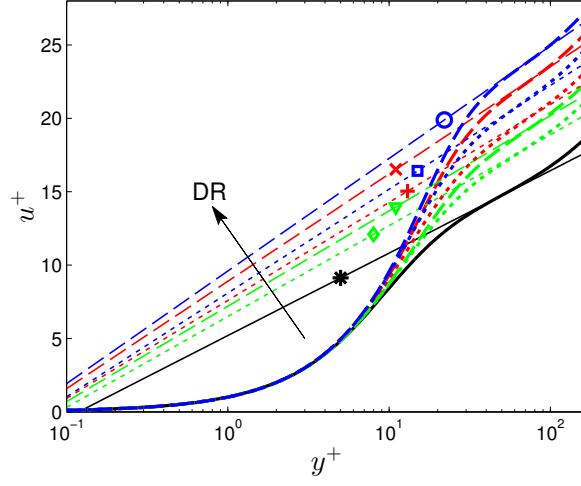


Figure 1: The velocity profiles scaled with actual friction velocity u_τ . Thick lines from DNS data; Thin lines (with symbols as in Table 1) according to Eq. (9). (—) Reference case; (— —) Spatial forcing; (· · ·) Temporal forcing. Color online: wall forcing amplitude $W_m^+ = 6$ (green); $W_m^+ = 12$ (red); $W_m^+ = 17$ (blue).

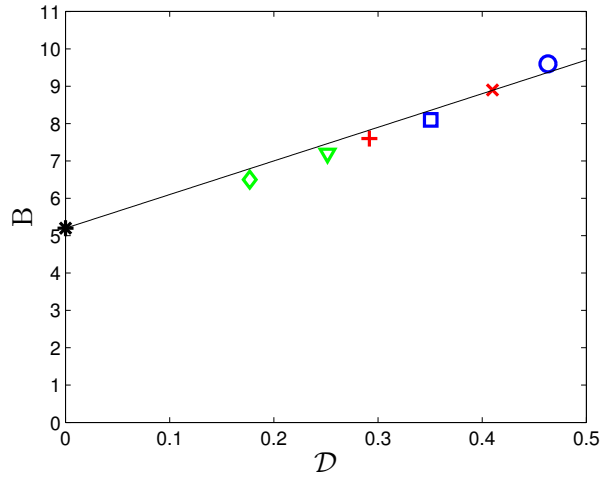


Figure 2: The additive constant B as a function of DR. The solid line is Eq. (16). Color online as in Fig. 1. Symbols as in Table 1.

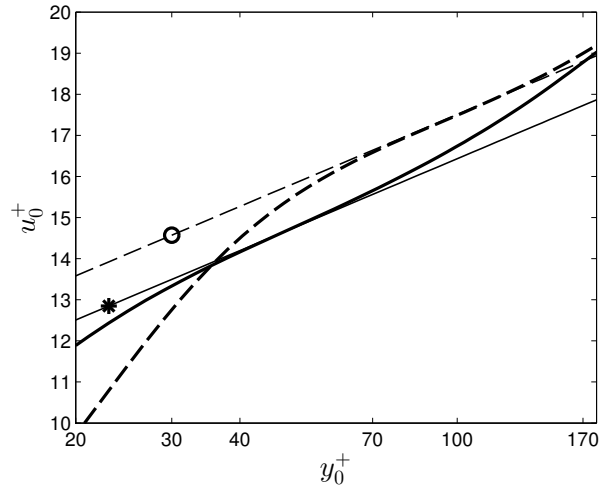


Figure 3: The velocity profiles in the logarithmic region scaled with reference friction velocity u_τ^0 . Thick lines from DNS data; Thin lines (with symbols as in Table 1) according to Eq. (10). (—) Reference case; (– –) Spatial forcing, case 6.

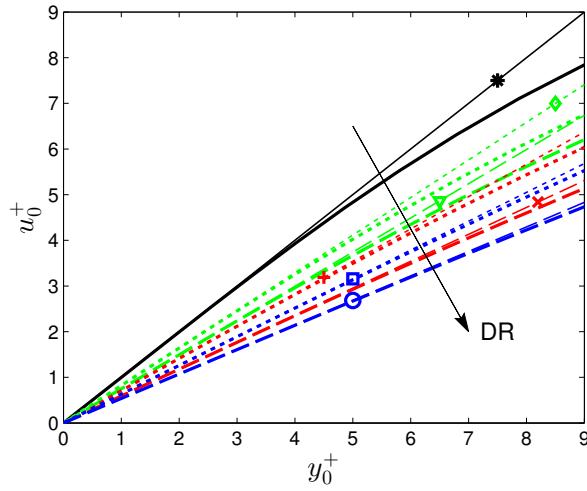


Figure 4: The velocity profiles in the linear sub-layer scaled with reference friction velocity u_τ^0 . Thick lines from DNS data; Thin lines (with symbols as in Table 1) according to Eq. (13). (—) Reference case; (– –) Spatial forcing; (\cdots) Temporal forcing. Color online: wall forcing amplitude $W_m^+ = 6$ (green); $W_m^+ = 12$ (red); $W_m^+ = 17$ (blue).

For the inner part it was already demonstrated in Fig. 1 that the relation (11) holds for all DR cases. When scaled with u_τ^0 the profiles can be compared to the equivalent relation (13). The velocity profiles from the DNS data are shown in Fig. 4 together with expression (13). In addition to the good agreement, we also note that the DNS data follows Eq. (13) further up (larger values of y_0^+) for larger values of \mathcal{D} , in agreement with the general conclusion that the viscous sub-layer is thickening when DR is achieved.

4. Verification with other data

So far in the present investigation, the comparison has only been made with low-Re DNS data (the oscillations commence at $Re_\Theta = 505$). In the following, verification of the results will be made by utilizing experimental results. When using experimental data for this purpose, care must be taken so that the friction velocity is not assumed to yield a logarithmic profile with a certain slope, rather the friction velocity should be determined utilizing the linear near-wall region. One such data set is obtained from Choi and Clayton (2001) who used a water tunnel boundary layer at $Re_\Theta = 1190$. The reference case and the most extreme DR case ($\mathcal{D} = 0.46$) are shown in Fig 5 (filled circles and empty squares, respectively). As can be clearly seen, the experimental profile experiences an identical change in the slope of the logarithmic part as predicted by the theoretical expression (9) shown as the solid line.

Additional data using the experimental investigation of a boundary layer at $Re_\Theta = 1400$ by Ricco and Wu (2004) is presented in Fig 5 as well. Also this set of data at three times higher Re (compared to the 6 DNS cases) follows the expression (9).

Next, the theory is compared with DNS of channel flow. In this case, the relation $Re_\tau = 1.13 \times Re_\Theta^{0.843}$ given by Schlatter and Orlu (2010) is used to convert the Re_τ used in channel flow configuration to Re_Θ used here. In Fig 5 the channel DNS by Toubert and Leschziner (2012) at $Re_\Theta = 1374$ is shown, as well as channel DNS by Quadrio et al. (2009) at $Re_\Theta = 464$. The latter simulation is performed with a combination of (14) and (15) forming a travelling wave forcing. Both of the channel flow DNSs seem to partially confirm the theory, albeit less convincing (most notably for case 9) than the boundary layer cases. We shall discuss this discrepancy in greater detail in the next section. All the cases used in Figs. 5 and 6 are summarized in Table 2.

The additive constant for all the experimental profiles (there are four DR cases provided in Choi and Clayton (2001)) are shown in Fig 6. The values of \mathcal{D} are not given in Choi and Clayton (2001) but are calculated using a mean of the top five points of measured velocity profiles, and are found to be 0.13, 0.26, 0.34 and 0.46 for the four cases (shown as \square in Fig. 6). The slight but systematic deviation between the actual values of B and what expression (16) yields, indicates a Re-dependence of the parameter k_D in (16), although weak due to the small difference in Re between DNS and experiment. This dependency comes as no surprise since B_0 (and even the κ in (8) for the canonical

Case	Type	Flow	Re_{Θ}	\mathcal{D}	symbol	line
7	experiment	boundary layer	1190	0.0-0.46	●; □	
8	experiment	boundary layer	1400	0.25	○	
9	DNS	channel	1374	0.32	+	...
10	DNS	channel	464	0.48	△	--

Table 2: Summary of the additional cases investigated. Symbols and lines are used in Figs. 5 and 6. Case 7 is taken from Choi and Clayton (2001), case 8 is taken from Ricco and Wu (2004), case 9 is taken from Touber and Leschziner (2012), and case 10 is taken from Quadrio et al. (2009).

turbulent boundary layer) is Re-dependent and is currently not fully determined (see for example the investigation by Schlatter et al. (2010)).

In order to further strengthen the argument that higher Re leads to lower values of B we utilize the additional data (cases 8-10 described in Table 2) in Fig. 6. Indeed, cases with higher Re ($Re_{\Theta} \approx 1400$), indicated by symbols + and ○ in Fig. 6, exhibit lower values of B compared both with the simulations at $Re_{\Theta} = 505$ (which is indicated as the straight line according to Eq. (16) in Fig. 6) and the experiments at $Re_{\Theta} = 1190$ (indicated with □), while the lower Re case at $Re_{\Theta} = 464$ (indicated with △) yields a slightly larger value.

Thus, all sets of data (at least the boundary layer data) agree with the theory regarding the slope of the logarithmic part of the velocity profile, and in addition, they show consistent behaviour with respect to the additive constant B . The slight deviation between the theory and channel flow DNS (case 9) is discussed next.

5. Range of validity of the theory

The theory presented is based on the assumption that the classical theory holds (only the inner part of the boundary layer is affected by the wall manipulations). If, in contrast, it is assumed that the outer part will eventually (sufficiently far downstream) adjust to the new conditions at the wall, the wake flow will, after reaching this new equilibrium, scale with the new friction velocity. As a consequence, the theory reverts to the normal logarithmic layer with a slope of $1/\kappa$. At this point the “old” friction velocity is not part of the equations and the boundary layer has lost all memory of its previous uncontrolled state.

However, no boundary layer simulation or experiment is close to being long enough to capture this effect. On the other hand, for the channel flow geometry the entire wall is oscillating, and hence the effect would manifest itself as a (slow) temporal transient where the slope reduces from $1/\kappa r$ to $1/\kappa$.

Returning to the lack of (perfect) agreement between the theory and channel DNS, one may note in Fig. 5 (focusing on case 9) that the logarithmic layer has a steeper slope than the reference profile in accordance with the theory. On the other hand, the theory overpredicts the slope which can be concluded from the observed steeper slope of the theoretical curve as compared with the DNS profile.

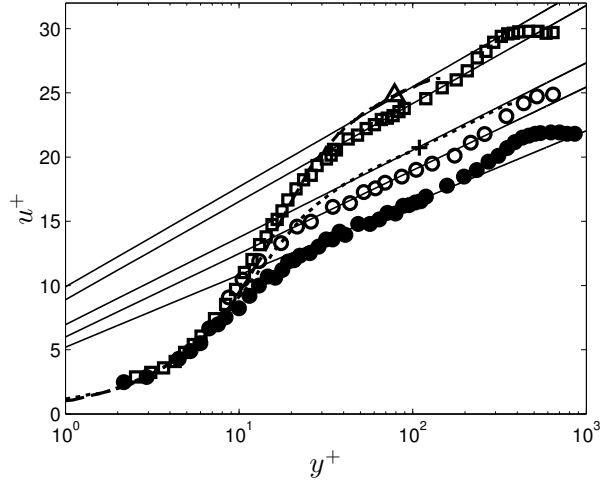


Figure 5: Velocity profiles scaled with actual friction velocity u_τ . Experimental data taken from Choi and Clayton (2001): ● Reference case; □ DR case with $\mathcal{D} = 0.46$. ○ Experimental data taken from Ricco and Wu (2004). ··· (+) DNS data taken from Touber and Leschziner (2012). - - (Δ) DNS data taken from Quadrio et al. (2009). Thin solid lines according to Eq. (9).

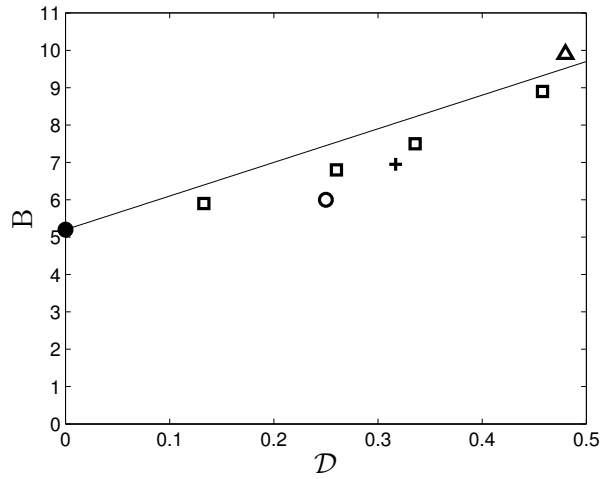


Figure 6: The additive constant B as a function of DR. ● Reference case at $Re_\Theta = 1190$; □ DR cases at $Re_\Theta = 1190$. ○ at $Re_\Theta = 1400$; + at $Re_\Theta = 1374$; Δ at $Re_\Theta = 464$. The solid line is Eq. (16) for $Re_\Theta = 505$.

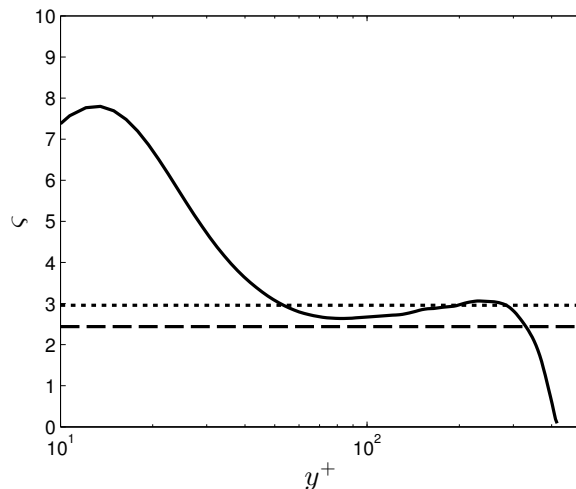


Figure 7: The indicator function, $\zeta = y^+ du^+ / dy^+$. (—) DNS data from Touber and Leschziner (2012); (···) Line indicating the value $1/\kappa r$; (---) Line indicating the value $1/\kappa$.

In order to show this more clearly and quantitatively, the indicator function, $\zeta = y^+ du^+ / dy^+$, is computed in Fig. 7. The local minimum of ζ indicates the slope of the logarithmic layer and is observed to be located between the original value ($1/\kappa$) and the theoretical value ($1/\kappa r$). This could be an indication that the simulation is long enough (in time) for the temporal transients (in the outer part) to start decaying. As a consequence of the readjustment of the outer part, the slope will eventually revert to $1/\kappa$. That the temporal transients have decayed in the channel flow DNS while the corresponding spatial transient still persists in the boundary layer is easily understood since the former is performed over typically around 20 periods while the latter has been limited to a spatial domain of around 4 periods (with a conversion between temporal and spatial domain by a convective velocity of 10 viscous units).

Note that the speculations presented in this section by no means invalidate any of the results previously reported in the referenced work from which the data is taken since all of the analysis presented in those works is performed on the near-wall region where the adjustment to the new wall conditions is much more rapid (1 to 2 periods) compared to the slow transients governing the outer wake flow discussed here.

6. Conclusions

A theory is presented which qualitatively predicts the slope which gradually increases with higher DR, in the case of wall oscillation induced DR.

The inner part of the turbulent boundary layer is responding directly to the wall oscillation and the velocity profiles is therefore governed by the new (actual) friction velocity, leading to $u^+ = f(y^+)$: Eq. (11). On the other hand, the outer part is unaffected by the oscillation and is consequently governed by the original friction velocity u_τ^0 , leading to that the matching procedure yields a profile depending on both velocity scales, in the form of either $u^+ = f(y^+, r)$: Eq. (9), or $u_0^+ = f(y_0^+, r)$: Eq. (10). Data from six DNSs have been shown to agree with the theoretical results. In addition, data from four independent investigations found in the literature support the theoretical results regarding the slope of the velocity profile. Furthermore, all the presented here consistently support the trend of lower values of the intercept B for increasing Re .

The following additional properties of the velocity profile have been derived theoretically and shown to comply with the DNS and experimental data:

- **In the logarithmic region:** Apart from the upward shift, also the slope is altered, when scaled with actual friction velocity. The slope becomes $1/(\kappa r)$. Furthermore, the intercept of the log-law depends linearly on the DR (or, equivalently, r^2). On the other hand, the slope of $1/\kappa$ is retained and the velocity profiles are closer to the reference case when scaled with the reference friction velocity.
- **In the linear region:** When scaled with reference friction velocity, the slope of the linear profile is changed from unity to r^2 .

Note that while the first point is unique for DR from oscillating walls, and is presented here for the first time, the second point is in common with all DR flows, and is of course not new.

The limitations of the presented study are the following: Only wall forcing of the type expressed by Eqs. (14) and (15) and their combination in the form of travelling waves have been considered when comparing the theory with data. However, for other types of wall manipulations for DR, such as riblets, the DR is too small for any detectable change in the slope of the logarithmic profile. Furthermore, fluid property changing methods, such as polymeric fluids or bubbly flow, result in more complicated DR mechanisms including non-Newtonian effects which are not included in the present analysis.

In addition, the comparison is only made with low- Re data (DNS and experiment). The values of B and hence the expression (16) will depend on the Re . However, similarly as concluded from the analysis of polymeric DR by White et al. (2012), the determination of the precise form of the dependency will have to wait until high-fidelity data of high- Re boundary layer profiles are available.

Finally, the theory has only been shown to predict the slope correctly for boundary layer flow at a relatively short distance from the onset of the oscillations (since no data exist for longer streamwise region of controlled flow). A question one might ask is, if a sufficiently long spatial extent of the wall forcing is allowed, will also the wake function be affected (i.e. will the classical theory be invalidated) for these high-DR cases? The experiments and simulations

of boundary layers performed to date are much too short (in the streamwise direction) for any conclusions regarding this to be drawn.

In addition, the agreement is less obvious for the channel flow, which may be due to that the wake region is affected and, as a consequence, the outer velocity scale is deviating from the nominal friction velocity. The reason this could occur in channel flow is that the entire wall is oscillating, and the temporal transients in the region far away from the wall are allowed to decay (to a certain degree) during a simulation. In contrast, the corresponding spatial transients in a boundary layer flow would require a much longer spatial domain than what is possible with the simulation tools available presently. Hence, the outer part has not yet adjusted to the new conditions imposed by the wall-control, leading to the two separate velocity scales on which the theory presented herein is based.

Thus, the slope of the logarithmic part of the velocity profile could serve as a measure of how well the outer part of the flow has adjusted to the imposed wall forcing.

7. Acknowledgments

Academic Research Fund Tier 2 (Grant No. MOE2012-T2-1-030) from Ministry of Education, Singapore, is greatly acknowledged.

Many thanks go to Dr. Emile Touber for sharing the DNS data.

References

- Choi, K.S., Clayton, B.R., 2001. The mechanism of turbulent drag reduction with wall oscillation. *Intl J. Heat Fluid Flow* 22, 1–9.
- Clauser, F.H., 1956. The turbulent boundary layer, Elsevier. volume 4 of *Advances in Applied Mechanics*, pp. 1 – 51.
- Duque-Daza, C.A., Baig, M.F., Lockerby, D.A., Chernyshenko, S.I., Davies, C., 2012. Modelling turbulent skin-friction control using linearized navierstokes equations. *J. Fluid Mech.* 702, 403–414.
- Elbing, B.R., Mäkiharju, S., Wiggins, A., Perlin, M., Dowling, D.R., Ceccio, S.L., 2013. On the scaling of air layer drag reduction. *J. Fluid Mech.* 717, 484–513.
- García-Mayoral, R., Jiménez, J., 2011. Drag reduction by riblets. *Phil. Trans. R. Soc. A* 369, 1412–1427.
- Karniadakis, G.E., Choi, K.S., 2003. Mechanisms on transverse motions in turbulent wall flows. *Annu. Rev. Fluid Mech.* 35, 45–62.
- Luchini, P., 1996. Reducing the turbulent skin friction, in: Desideri, J.A., Hirsch, C., Le Tallec, P., Oñate, E. (Eds.), *Computational Methods in Applied Sciences 1996*. Proc. 3rd ECCOMAS CFD Conference, pp. 466–470.

- Min, T., Kang, S.M., Speyer, J.L., Kim, J., 2006. Sustained sub-laminar drag in a fully developed channel flow. *J. Fluid Mech.* 558, 309–318.
- Moarref, R., Jovanović, M.R., 2012. Model-based design of transverse wall oscillations for turbulent drag reduction. *J. Fluid Mech.* 707, 205–240.
- Nakanishi, R., Mamori, H., Fukagata, K., 2012. Relaminarization of turbulent channel flow using traveling wave-like wall deformation. *Intl J. Heat Fluid Flow* 35, 152 – 159.
- Quadrio, M., 2011. Drag reduction in turbulent boundary layers by in-plane wall motion. *Phil. Trans. R. Soc. A* 369, 1428–1442.
- Quadrio, M., Ricco, P., Viotti, C., 2009. Streamwise-travelling waves of spanwise wall velocity for turbulent drag reduction. *J. Fluid Mech.* 627, 161–178.
- Ricco, P., Wu, S., 2004. On the effects of lateral wall oscillations on a turbulent boundary layer. *Exp. Therm. Fluid Sci.* 29, 41–52.
- Schlatter, P., Li, Q., Brethouwer, G., Johansson, A.V., Henningson, D.S., 2010. Simulations of spatially evolving turbulent boundary layers up to $Re(\theta)=4300$. *Intl J. Heat Fluid Flow* 31, 251–261.
- Schlatter, P., Orlu, R., 2010. Assessment of direct numerical simulation data of turbulent boundary layers. *J. Fluid Mech.* 659, 116–126.
- Skote, M., 2011. Turbulent boundary layer flow subject to streamwise oscillation of spanwise wall-velocity. *Phys. Fluids* 23 (081703).
- Skote, M., 2012. Temporal and spatial transients in turbulent boundary layer flow over an oscillating wall. *Intl J. Heat Fluid Flow* 38, 1–12.
- Skote, M., 2013. Comparison between spatial and temporal wall oscillations in turbulent boundary layer flows. *J. Fluid Mech.* 730, 273–294.
- Skote, M., Henningson, D.S., 2002. Direct numerical simulation of a separated turbulent boundary layer. *J. Fluid Mech.* 471, 107–136.
- Spalart, P.R., McLean, J.D., 2011. Drag reduction: enticing turbulence, and then an industry. *Phil. Trans. R. Soc. A* 369, 1556–1569.
- Tamano, S., Graham, M.D., Morinishi, Y., 2011. Streamwise variation of turbulent dynamics in boundary layer flow of drag-reducing fluid. *J. Fluid Mech.* 686, 352–377.
- Touber, E., Leschziner, M.A., 2012. Near-wall streak modification by spanwise oscillatory wall motion and drag-reduction mechanisms. *J. Fluid Mech.* 693, 150–200.
- Virk, P.S., 1975. Drag reduction fundamentals. *AIChE Journal* 21, 625–656.

- White, C.M., Dubief, Y., Klewicki, J., 2012. Re-examining the logarithmic dependence of the mean velocity distribution in polymer drag reduced wall-bounded flow. *Phys. Fluids* 24 021701.
- White, C.M., Mungal, M.G., 2008. Mechanics and prediction of turbulent drag reduction with polymer additives. *Annual Review of Fluid Mechanics* 40, 235–256.
- Yudhistira, I., Skote, M., 2011. Direct numerical simulation of a turbulent boundary layer over an oscillating wall. *J. Turbul.* 12, N9.